ID 174

Optimised rotor head design for an Economic Helicopter

T. Kneisch, R. Krauss, A. D'Alascio, D. Schimke
Aerodynamics
Eurocopter Deutschland GmbH
81663 Munich, Germany
e-mail: thomas.kneisch@eurocopter.com

The paper presents two different aerodynamic design exercises both having the final goal of reducing drag and increasing lift of a helicopter main rotor head. For the numerical investigations, the two flow solvers FLOWer and TAU, both developed by DLR, are applied to investigate a baseline configuration and several newly designed sub-variants. The comparison among the different configurations is made in terms of forces acting on hub components, as well as in terms of pressure distributions. Besides the aerodynamic design, the paper focuses also on different numerical modelling approaches, aiming at reducing the model complexity and the computational time. The paper concludes by listing advantages and limitations of the different computational approaches and giving an outlook of further investigations extending the understanding of rotor head aerodynamics.

INTRODUCTION

In line with the year 2020 goals set by ACARE (Advisory Council for Aeronautics Research in Europe) the European Technology Platform for Aeronautics & Air Transport, the helicopter manufacturers are committed to develop efficient aircrafts minimizing their negative impact on the environment. A key role in this technical area is the reduction of overall helicopter drag since this directly decreases the helicopters' fuel consumption and accordingly emissions in level flight. Considering that up to a third of the total drag of a light or medium helicopter can be attributed to its rotor head, more and more attention has been given lately (see [2] and [3]) to the aerodynamic improvement of this component.

Beside experimental investigations, numerical methods, such as Computational Fluid Dynamics (CFD), are applied with growing extend in the industrial design process at Eurocopter. The numerical tools give deep insight on local fluid quantities and allow visualizing the fluid flow helping the aerodynamic engineer to understand complex flow phenomena. Furthermore, CFD allows adapting the complexity of the model - from simple 2- to complex 3-dimensional setups - and consequently the numerical effort to answer specific engineering requests.

CFD, applied in combination with Computer Aided Design (CAD) tools for the 3D surface modelling, enables the aerodynamic engineer to modify the surface definition, searching for aerodynamic improvements, without violating structural and geometrical constraints: the combination of these methods allows for a concurrent aerodynamic and structural design of helicopter components.

NUMERICAL APPROACH

Code Description

Within the context of the numerical investigations of the rotor head described in this paper both flow solvers developed at DLR – FLOWer, following a multi-block structured approach and TAU, using an unstructured method - are used. A general description of the flow solvers is given in [1], [6] and [7] for FLOWer and [4] and [5] for TAU.

FLOWer:

The flow solver FLOWer solves the compressible three-dimensional unsteady Reynolds-averaged Navier-Stokes equations (URANS) on structured multiblock grids. The spatial discretisation is based on a cell-centred finite volume formulation with artificial dissipation, whereas the time discretisation is implemented through a 5-stage Runge-Kutta scheme. Local time stepping, implicit residual smoothing and the multigrid method are used to accelerate convergence. Complex helicopter applications with rotating bodies are supported by a fully general motion module, a grid deforming module, which is not used for the investigations of this paper, and the implementation of the Chimera Technique using overlapping sub-grids. Turbulence is modelled by different algebraic or advanced multi-equation transport models as for instance the 2-equation Wilcox k-ω, which is used for the FLOWer simulations in this paper.

TAU:

The TAU code solves the URANS equations on unstructured grids featuring the four primary cell element types: tetrahedral, hexahedra, prism and pyramid. The method used for the investigation is a cell-vertex finite volume formulation with an implicit Backward-Euler time-stepping scheme. TAU provides a series of different turbulence models, ranging from algebraic to multi-equation transport models, whereas all TAU simulations described in the present paper are performed with the 2-equation Menter-SST model. Convergence acceleration is enabled by local time stepping, residual smoothing and the multigrid method. Arbitrary body translation and rotation is employed by a general motion module as well as the Chimera technique.

<u>The 5-blade isolated bearing-less main rotor head</u>

The focus of the investigation is set on a full-scale 5-bladed bearing-less main rotor head similar to the ATR-3 rotor head design. The rotor head features a blade folding mechanism. The folding capability, which allows for a smaller hangar area to park a helicopter, has the drawback of reducing the effective rotor blade area.

Case description

Since the drag reduction of the rotor head and particularly of its blade necks is the main goal of the present investigation, a fast level flight at 140knots at 5000ft ISA conditions is selected for the analysis. For all simulations the helicopter attitude, the rotor mast inclination and rotational speed, as well as collective and cyclic pitch motion of the rotor blade necks, are prescribed, if not explicitly stated differently in the text or figures. The pitch motion is kept identical for all computations and during each computation, so that always the same helicopter trim is used. The rotor blade lead lag and flap motions have been neglected in all computations. Table 1 summarizes the setup of the simulations.

Table 1: 5-bladed isolated rotor head: computational setup

atmospheric condition	5000ft ISA
flight velocity	140kts
helicopter angle of attack	-1.5deg
helicopter yaw/ roll angle	0.0deg
rotor mast inclination	-5.0deg
rotor rotational speed	35.714rad/sec

Model geometry

In the context of the investigation of the isolated 5-bladed bearing-less main rotor head an additional study is performed to investigate the determination of the aerodynamic loads on the rotor blade neck with a simplified 1-blade setup instead of the normally used complete 5-blade configuration. Therefore two different geometry configurations are described in the following:

5-blade configuration

Figure 1 shows the simplified 5-blade geometry of the baseline rotor head. The model features the rotor head mast, hubcap and blade necks with the upper and lower lead lag dampers, the rotor blade attachment (pink component (Part 04) in Figure 1) as well as the radial inner part of the main rotor blade. Components of the drive system, e.g. pitch rods and swash plate, the flexbeam, blade bolts, as well as the helicopter fuselage, are neglected. Such an assumption is possible since the comparison of the rotor blade necks among each other is the focus of the investigation and not the determination of the rotor head total loads.

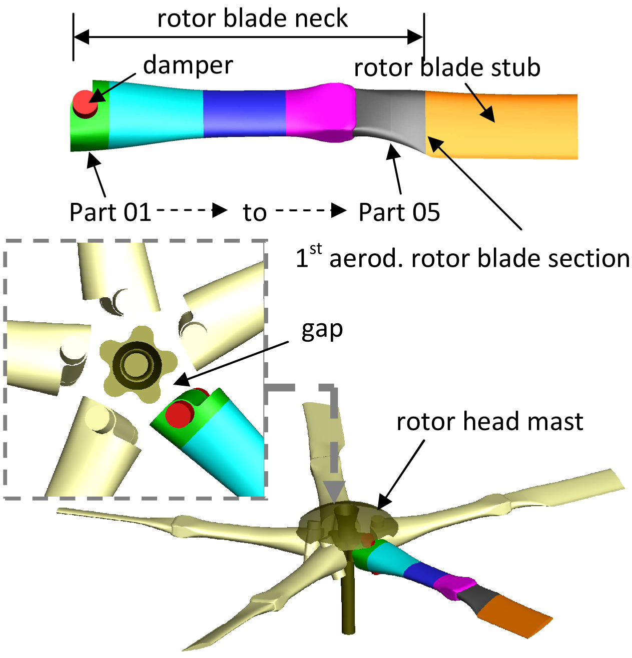

Figure 1: 5-blade configuration of the isolated bearing-less rotor head geometry

Particularly the fuselage elements placed upstream of the rotor head, e.g. nose and swash plate fairing, influence the direction of the flow impinging the rotor head; therefore the determination of the global loads would not be fully reliable. As indicated in Figure 1 by different surface colouring - exemplarily shown for one of the rotor blade necks - the complete geometry is subdivided for the simulation in different sub-components, so that a detailed aerodynamic load breakdown can be determined. The rotor blade neck is subdivided in Part 01 to Part 05 numbered from radial inboard to outboard.

1-blade configuration

For the 1-blade configuration four of the five rotor blade necks are omitted so that only one rotor blade is rotating with the rotor head mast around the rotor axis. The geometry of mast and rotor blade neck of the 1-blade configuration is identical to the 5-blade configuration.

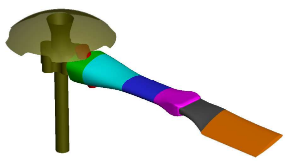

Figure 2: 1-blade configuration of the isolated bearing-less rotor head geometry

Rotor blade neck variants

Figure 3 shows the different rotor blade neck variants, which are investigated. The respective geometry of the rotor blade neck is based on a general parametric CATIA V5 CAD model allowing the modification of radial cross sections, twist and chord in the area between pitch horn and the first aerodynamic main rotor blade section.

Variants A to C feature a fully aerodynamically faired rotor blade attachment, whose cross section is based on a thickness-adapted NACA airfoil. Variants A to C also feature the identical twist distribution, which is different to the twist definition of the baseline configuration. For Variant B, the adapted NACA airfoil is used for the fairing of the rotor blade attachment (Part 04). In the transition area to the pitch horn (Part 01) an elliptical cross section is used instead and the plan view is kept similar to the baseline rotor blade neck. For Variant A, the adapted NACA airfoil is used in the complete transition region between the rotor blade attachment and the pitch horn, so that the rotor blade neck features a blunt trailing edge. As shown in Figure 3 the plan view is modified so that a smooth transition to the rotor blade is achieved. Variant C combines the plan view of Variant A and the application of the elliptical cross section in the radial inboard area of the rotor blade neck. In addition, the pitch horn and subsequently the transition to Part 04 is created with a larger height of construction as the other variants.

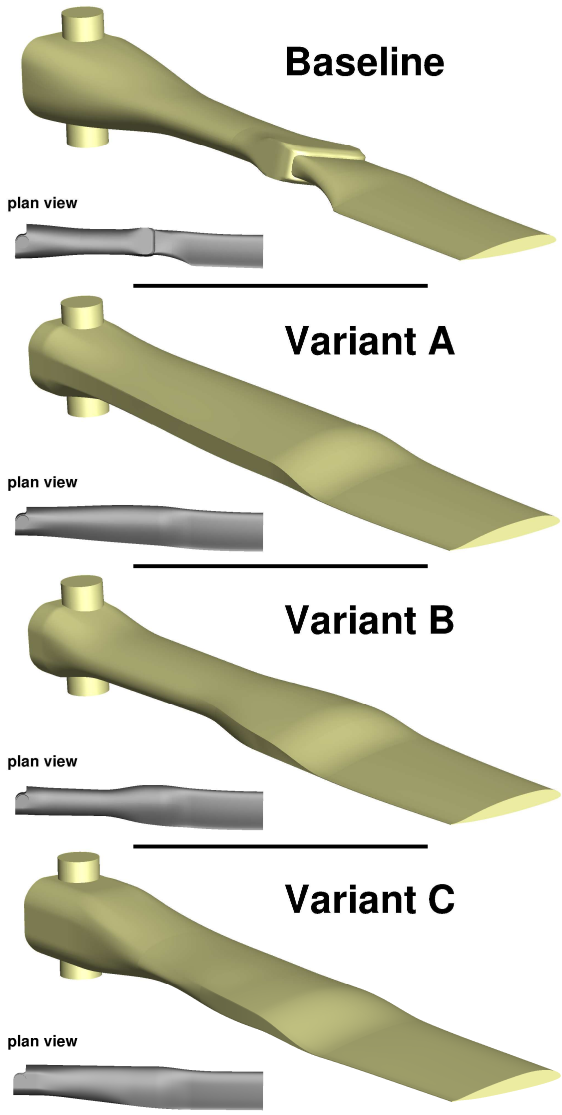

Figure 3: rotor blade neck variants

The geometry of the rotor blade neck is subjected to different constructive and operational constraints. The minimum thickness of the radial cross sections of the rotor blade neck for example is limited by the structural strength of the respective load-bearing components. Requirements concerning the clearance between rotor blade neck and adjacent components like flexbeam and rotor mast have to be respected when the outer surface of these elements is defined. Furthermore other design aspects like the dynamic layout of the rotor in terms of bending and torsion stiffness in the area of the rotor blade neck as well as requirements of a rotor blade folding mechanism affect its geometrical design.

Grid System

For the complete study, a chimera grid system with a set of overlapping structured multiblock-grids around the geometry is build (see Figure 4 and Figure 5): the father (background) mesh, a body-fitted grid generated around the rotor mast and hubcap, which models also the outer computational domain, contains body fitted meshes generated around each rotor blade neck. During the computation the flow information is exchanged between the meshes at each time step by the chimera interpolation module of FLOWer. For the generation of the sub-grids the commercial grid generator ICEMCFD Hexa of ANSYS is used.

The Chimera grid system for the 1-blade and the 5-blade configuration consists of identical sub-grids. The 5-blade configuration combines the rotor head and background grid with 5 grids of the rotor blade neck. In this way the grid system consists of 370 blocks and 10.17×10^6 nodes. The 1-blade configuration features the rotor head grid and one rotor blade neck grid, thus consisting of 146 blocks and 5.41×10^6 nodes.

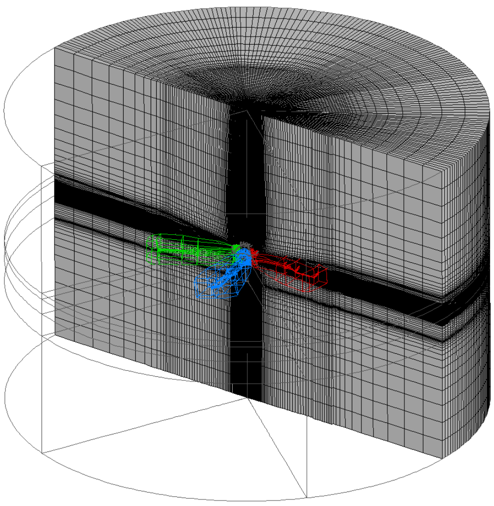

Figure 4: : 5-bladed isolated rotor head: Chimera grid system of the 5-blade configuration

For both configurations the outer mesh boundary is located 2.5 times the outer radius of the rotor blade stub below and above the rotor plane. The radius of the cylindrical mesh domain corresponds to 3.75 times the outer radius of the rotor blade stub. A detailed grid statistic for the respective sub-grids is summarized in Table 2.

Table 2: 5-bladed isolated rotor head: grid statistics

	No. of sub-grids	blocks	nodes [$\times 10^6$]
mast & hubcap & background grid		90	4.22
blade neck grid		56	1.19
SUM 1-blade configuration	2	146	5.41
SUM 5-blade configuration	6	370	10.17

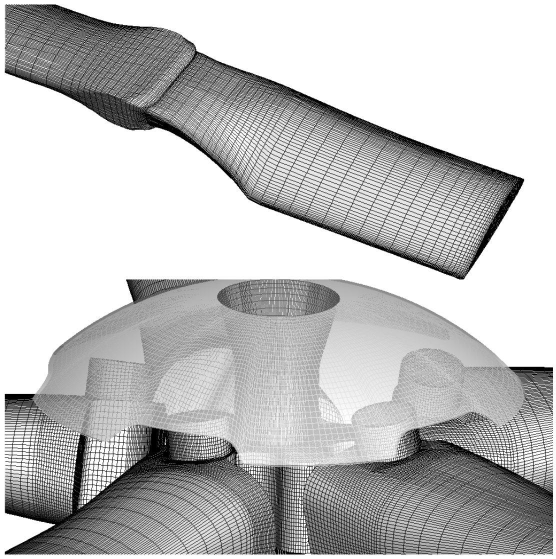

Figure 5: 5-bladed isolated rotor head: detail of surface grid of the 5-blade configuration

Discussion of the numerical results

Comparison 1-blade and 5-blade configuration

The comparison of the time-dependent aerodynamic loads for one single rotor blade neck in terms of drag, lift and power - all determined by the integration of pressure and friction forces on the respective elements - is shown in Figure 6 for the baseline configuration and Variant C (for some configurations the results are only shown up to azimuth position = 1080°). The horizontal axis of the diagrams describes the azimuth position ψ of the rotor blade neck, whereas ψ=0°, 360°, 720°, etc. correspond to the main helicopter direction with the rotor blade neck directing from helicopter nose to the tail. The rotor blade neck at ψ=90°, 450°, 810° is directed to the right helicopter side (looking in flight direction) so that the rotor rotates anticlockwise (seen from the top). The aerodynamic loads shown in the figures are integrated for one rotor blade neck (blue coloured component in the upper left figure in Figure 6). The drag and lift are given in the wind-frame, whereas the power is specified in the tilted rotor head coordinate system. The outer rotor blade stub component is excluded for the comparison since it is influenced by the artificial tip vortex generated at the tip of the blade stub.

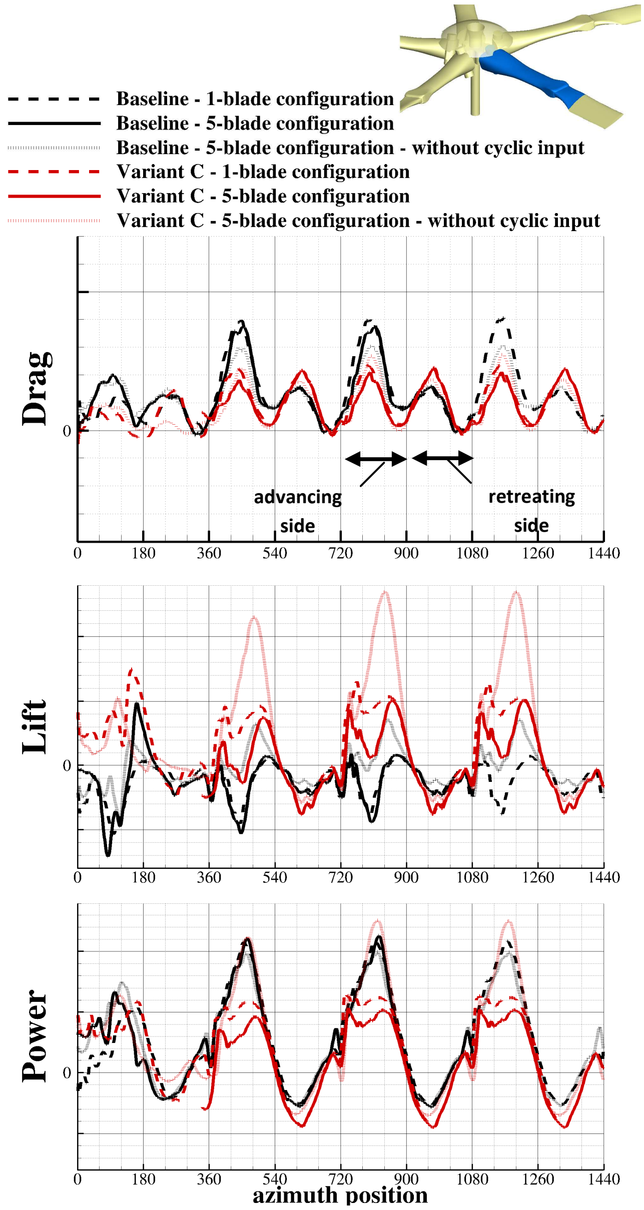

Figure 6: comparison of aerodynamic loads on one rotor blade neck: 1-blade and 5-blade configuration as well as with and without cyclic rotor blade pitch

The drag, lift and power curves versus azimuth position show similar trends for the baseline geometry within a complete rotor revolution. When the values of the 5-blade configuration are used as reference, the deviation of the time-averaged aerodynamic loads on one rotor blade neck between 1- and 5-blade configuration is 12% for the drag, 10% for the lift and 19% for the power required to rotate the rotor blade neck (see Figure 7 to Figure 9).

Performing the same comparison with the results of Variant C points out, that only the drag value is predicted similar by the two different approaches. The lift and power values manifest large differences, which occur especially on the advancing rotor blade side when one rotor blade neck is in the wake of the preceding one. Using the 5-blade configuration of Variant C as reference, the deviation of the averaged aerodynamic loads of one rotor blade neck between the two different modelling approaches is 10% for the drag, 205% for the lift and 72% for the power.

The difference of the lift is mainly caused by the different downwash generated in the rotor plane by the 1- and 5-blade configuration. With the 1-blade configuration the downwash of the four omitted rotor blades is missing, thus the effective angle of attack relative to the single rotating rotor blade is different. In this way, all rotor blade neck components of Variant C produce a larger lift in the 1-blade computation than in the 5-blade computation (see Figure 11). The different angle of attack of the approaching flow has a smaller impact on the drag values of the components since the drag value of the cross section with blunt trailing edge (ellipse and adapted NACA airfoil) is significantly less sensitive than its lift value in a wide range of angle of attack around 0deg. Preliminary 2D polar computations of the cross sections, which are not reported in this paper, have substantiated this behaviour. As shown in Figure 10, the different drag predictions for the rotor blade neck of the two modelling approaches can basically be assigned to the inner part (Part 01) of the rotor blade neck. Due to the vicinity of the rotor blade necks in the radial inboard region significant shadowing effects occur especially on the advancing rotor blade side reducing the drag of this element in the 5-blade computation. The same effect explains the different drag predicted for the rotor head mast. The rotor head mast creates less drag when one of the rotor blade necks is located in front of it (ψ=180°, 540°, etc.). In the 1-blade configuration this happens only once per revolution, therefore, the integral drag of one rotor revolution is higher.

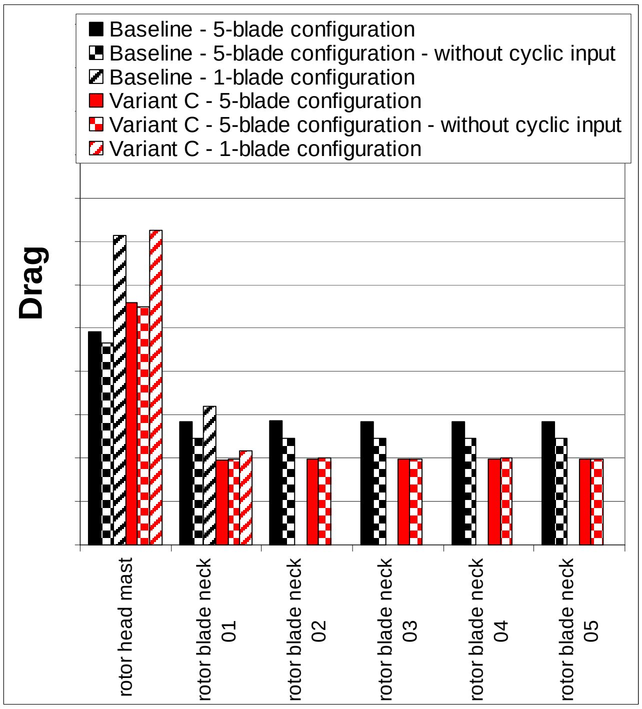

Figure 7: global drag breakdown (time-averaged quantities of one rotor revolution)

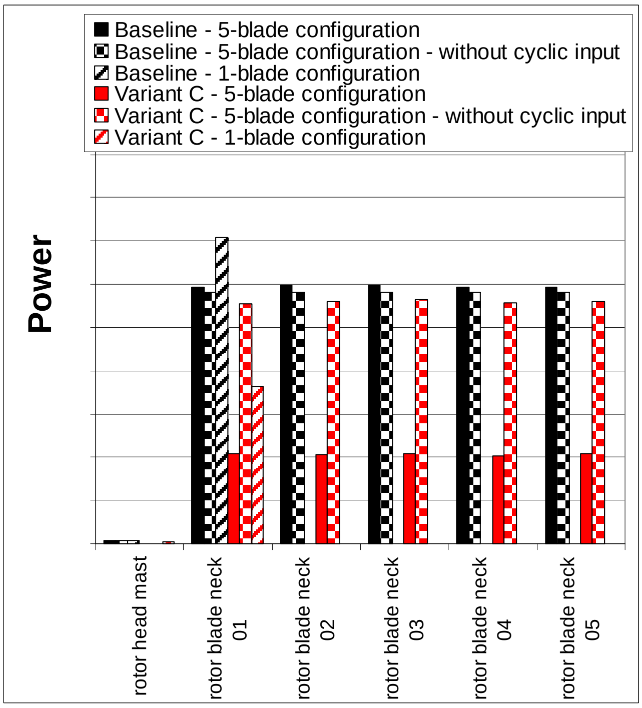

Figure 9: global power breakdown (time-averaged quantities of one rotor revolution)

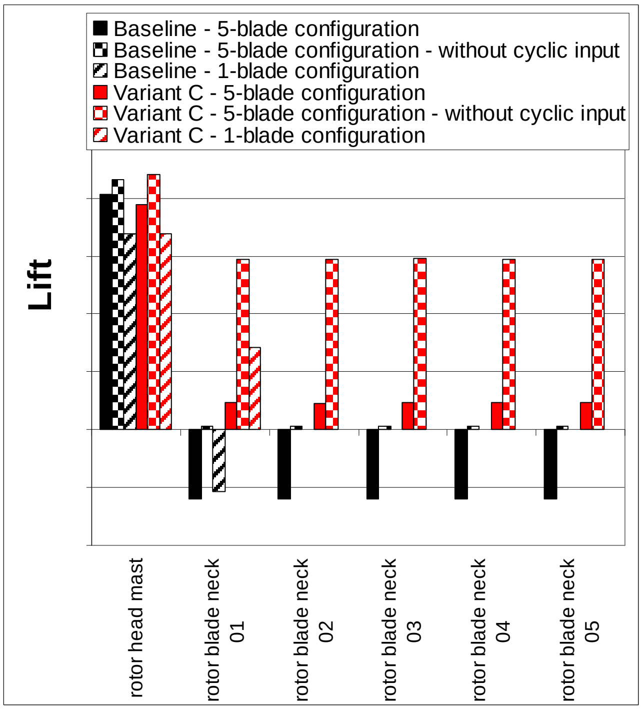

Figure 8: global lift breakdown (time-averaged quantities of one rotor revolution)

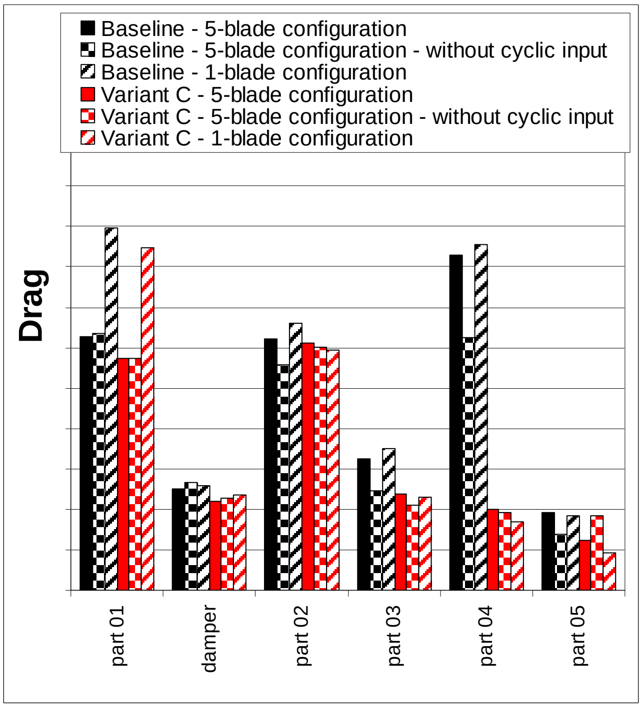

Figure 10: local rotor blade neck 01 drag breakdown (time-averaged quantities of one rotor revolution)

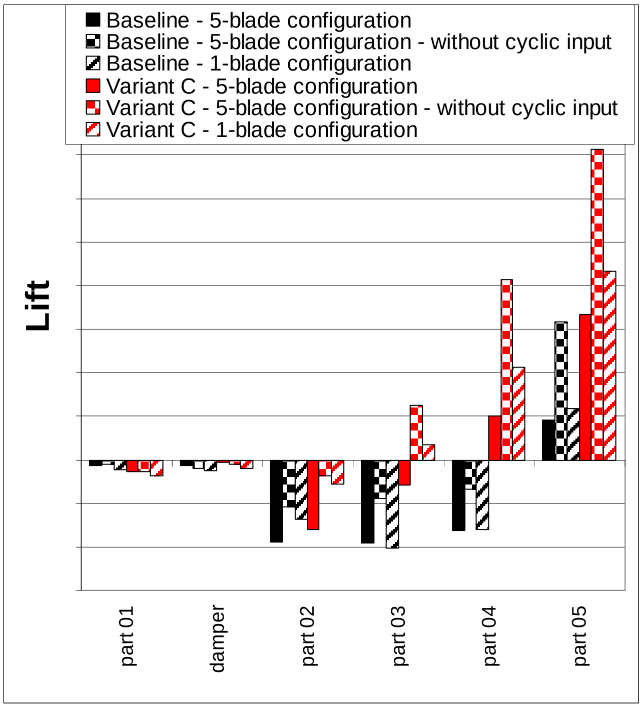

Figure 11: local rotor blade neck 01 lift breakdown (time-averaged quantities of one rotor revolution)

Figure 12 and Figure 13 show the pressure distribution and friction lines on the rotor head surface for the 1- and 5-blade computations of Variant C at the end of the third rotor revolution. In Figure 13 the respective time-steps of the unsteady 1-blade computation are superimposed so that the depicted rotor blade positions correspond exactly to the positions of the rotor blades of the 5-blade computation (azimuth offset is 72deg).

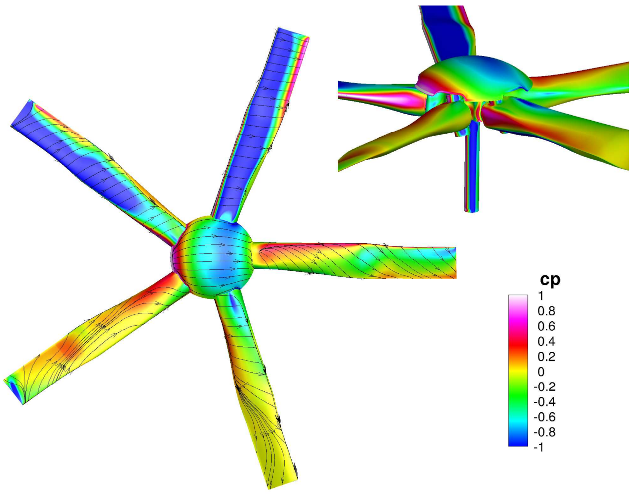

Figure 12: Variant C: pressure distribution and friction lines of the 5-blade configuration

The pressure distribution and friction lines on the hubcap correspond to the time-step of the rotor blade pointing to the right in Figure 13.

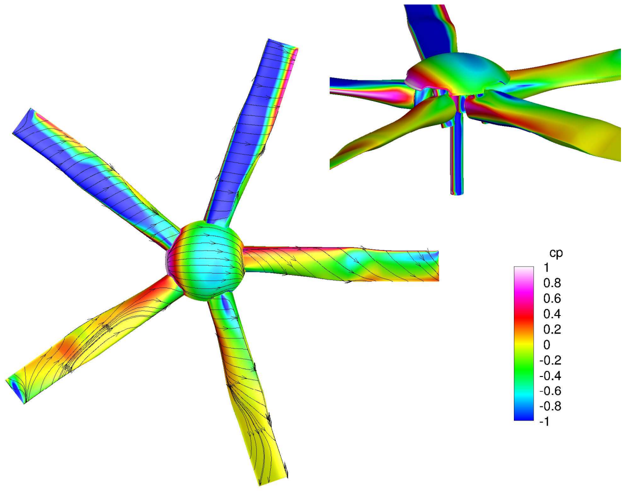

Figure 13: Variant C: pressure distribution and friction lines of the 1-blade configuration (superimposed time-steps of the unsteady computation with 72deg offset)

Drag analysis: 1-blade configuration

Figure 14 and Figure 15 show the results of the 1-blade computations in terms of aerodynamic drag that is generated by a single rotor blade neck (for some configurations the results are only shown up to azimuth position = 1080°). As shown in Figure 14, the high drag level on the advancing rotor blade side of the baseline configuration is reduced significantly by all other variants.

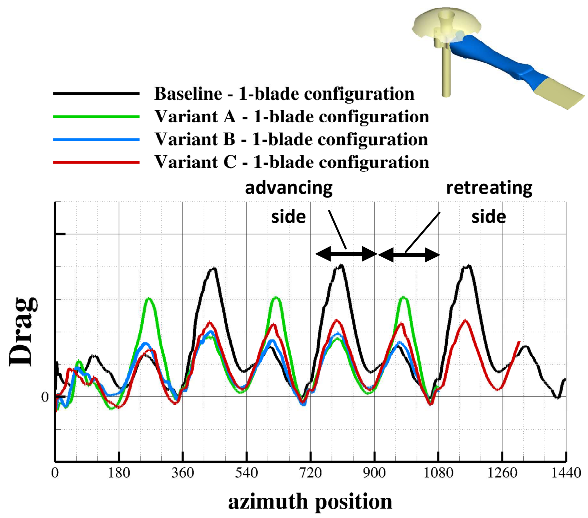

Figure 14: 1-blade configuration: time-dependant aerodynamic drag of the rotor blade neck variants

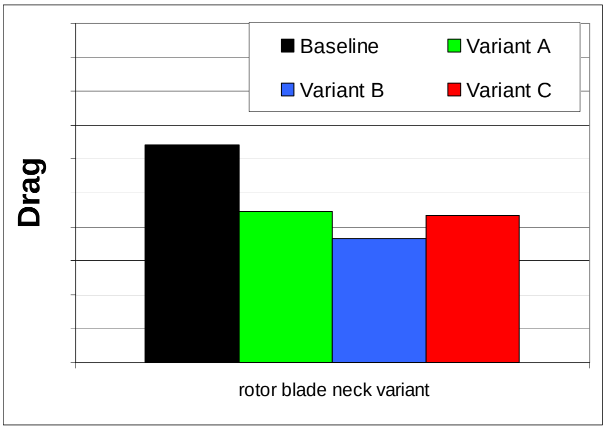

Figure 15: 1-blade configuration: time-averaged aerodynamic drag of the rotor blade neck variants

The main contribution to the drag reduction can be assigned to part 03, 04 and 05 as it is illustrated in Figure 16. The drag generated by the rectangular cross section is significantly higher than the drag generated by the adapted NACA airfoil cross section.

The high drag maxima on the retreating rotor blade side, which occurs particularly dominant at Part 02 and Part 03 of Variant A, is caused by the blunt trailing edge of this variant in this area. Due to the low rotational speed at the inner parts of the rotor head, the radial inner components are subjected to a velocity which corresponds approximately to the free stream velocity both on the advancing and retreating rotor blade side. In fast level flight this blunt shape contributes significantly to the overall drag of the rotor blade neck. The more outboard the position of the cross section, the lower the reverse flow velocity on the retreating rotor blade side and less severe the negative impact of the blunt trailing edge. As shown in Figure 16, the drag of Part 04 on the retreating rotor blade side is already very low since the reverse flow velocity is small. For the radial inboard area of the rotor blade neck the ellipse presents a compromise for both advancing and retreating rotor blade side, demonstrated by a similar drag value on the advancing and retreating side.

The increased geometrical height of the inner part of the rotor blade neck (Part 02) of Variant C causes an increased maximum drag value on the advancing and retreating rotor blade side compared to Variant B featuring a smaller height of construction.

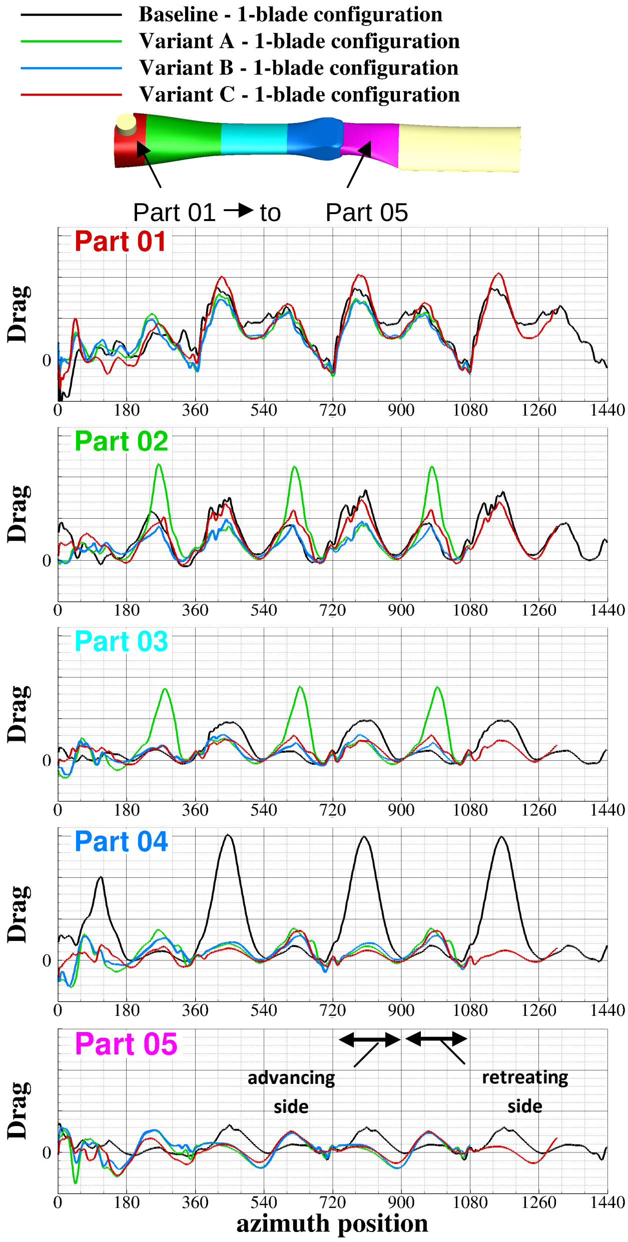

Figure 16: 1-blade configuration: time-dependant aerodynamic drag of different sub-parts of a single rotor blade neck

Analysis of the effect of the cyclic pitch motion on the aerodynamic loads of the rotor blade neck with the 5-blade configuration

The comparison of the time-dependant and time-averaged aerodynamic loads of the rotor blade neck for the computations with and without cyclic pitch motion of the rotor blades is shown in Figure 6 to Figure 11. The relation points out, that by omitting the cyclic pitch motion of the rotor blades, the drag of the rotor blade neck is predicted different at the two specific azimuth positions $\psi \approx 90$ and $\psi \approx 270$. Comparing the time averaged value of one rotor revolution shows only small differences (Baseline: 5% deviation, Variant C: 2% deviation). In contrast to that, the lift and the power manifest large differences especially on the advancing rotor blade side when the blade angle of attack is not reduced by the cyclic input.

Since the differences in the numerical setup with and without cyclic pitch motion of the rotor blades are very small and the computation time is identical to the computation with cyclic pitch motion, it is recommended to implement the cyclic pitch motion of the rotor blade necks in the rotor head simulation.

The 4-blade rotor head of the EC135

The second numerical investigation is carried out with the unstructured TAU solver. It aims at studying the effect on drag and lift of different hubcap modifications on the 4-bladed bearing-less main rotor head of the EC135 helicopter (see Figure 17).

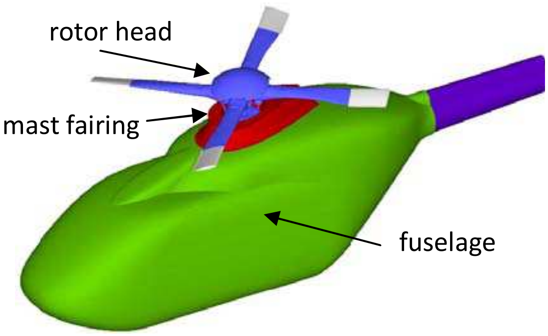

Figure 17: geometry of the EC135 cabin and rotor head

Geometry description

Taking as reference the EC135 serial hubcap, different hubcap designs are investigated in the study (see Figure 18 and Figure 19). Starting with configuration A, the general shape in terms of width, height and curvature of the hubcap is left unchanged compared to the reference hubcap, but the position is modified by moving the hubcap along the rotor axis by 55mm closer to the helicopter cabin. The cut-outs for the rotor blade necks, which are located at each rotor blade position, are adapted so that the clearance between rotor blade neck and hubcap is ensured. The hubcap of Configuration B is also positioned 55mm lower than the reference hubcap. In addition it features a 100mm larger diameter, whereby the curvature of the hubcap surface is reduced, since its height is kept unchanged. As depicted in Figure 19, Configuration C is defined by omitting the hubcap completely.

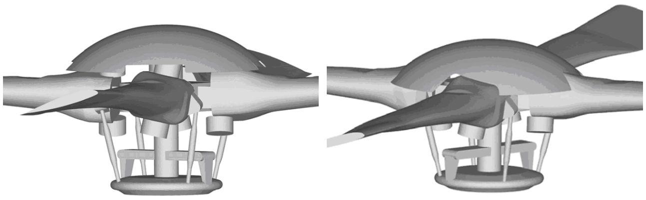

Figure 18: reference hubcap (left) – Configuration A with 55mm lower hubcap (right)

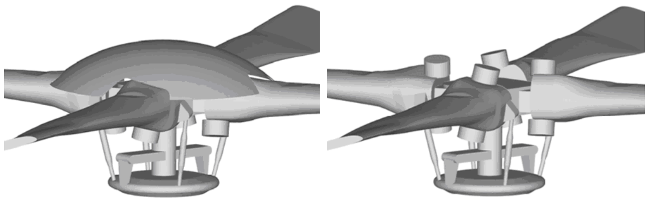

Figure 19: Configuration B with 55m lower and 100m wider hubcap (left) – Configuration C without hubcap (right)

Case description

A fast level flight with a flight velocity of 140kts in 5000ft ISA is selected for the analysis. The helicopter attitude is set to an angle of attack of -1.5deg without yaw and roll angle. The analysis is performed with the rotor head placed on a simplified model of the helicopters' fuselage in the 45deg-azimuth-position as it is shown in Figure 17. The empennage with Fenestron® and horizontal stabilizer is omitted, whereas the rotor head, on which the focus of the investigation is placed, is kept as detailed as possible, featuring elements like pitch rods, drive arms, dampers, pitch horns and the swash plate.

All computations are performed in steady state mode with non rotating rotor except one unsteady computation with the reference rotor head configuration. In all simulations the pitch, lead lag and flap motions of the rotor blade are not taken into account.

Grid system

For each configuration an unstructured chimera grid system is generated with ICEMCFD-Tetra/Prism of ANSYS by applying the Octree algorithm for the tetra generation. The respective grid system consists of two sub-grids; one including the fuselage geometry and the complete background – which is used for all chimera grid systems – and one including the respective rotor head geometry.

The mesh of the baseline hubcap configuration is depicted in Figure 20 and Figure 21. Especially in the area around the rotor head the grid is strongly refined to cover all details of the rotor head assembly.

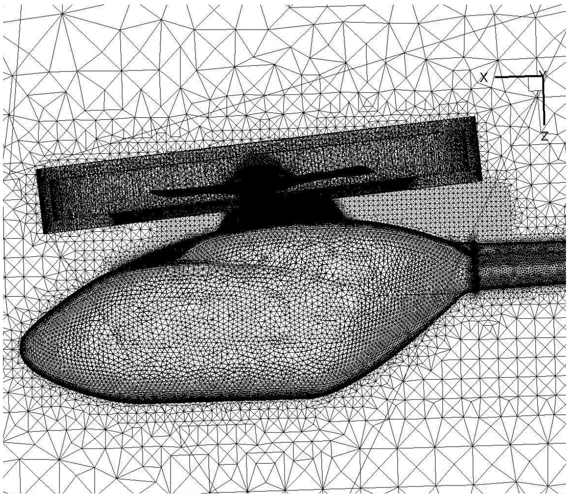

Figure 20: chimera grid system of the EC135 cabin and rotor head

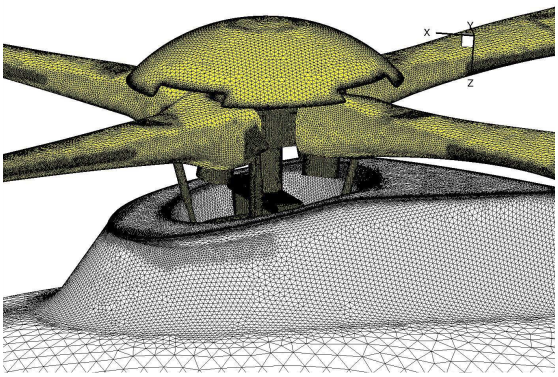

Figure 21: surface grid of the EC135 rotor head

Table 3 summarizes the overall grid statistics for all hubcap variants.

Table 3: The 4-blade rotor head of the EC135: grid statistics

grid	nb. of nodes [x10^6]
reference configuration	8.199
Configuration A	8.212
Configuration B	8.288
Configuration C	7.526

Discussion of the numerical results

The aerodynamic drag and lift breakdown of the rotor head and the mast fairing is depicted in Figure 22 and Figure 23. Due to the missing rotor head rotation in the steady state computations and the missing rotor blade pitch motion in all computations, the thrust, which is generated by the rotor blade necks along the rotor axis, is unrealistic and set to zero for all computations.

A comparison of the results of the simulation with the rotating rotor head and the ones with non rotating rotor head shows that the time-dependant lift and drag values within one rotor revolution differ especially on the blade necks. However the time-averaged forces of one rotor revolution are very similar on the components so that the design study is performed using the non-rotating rotor head approach (see Figure 22 and Figure 23).

The general aerodynamic effect of the hubcap can be seen by comparing the results of the reference configuration with the results of the configuration without a hubcap. The configuration without hubcap creates slightly less drag and significantly less lift compared to the reference configuration.

Lowering the hubcap by 55mm reduces the drag of the rotor head especially by covering more elements below the hubcap. The lift is only slightly decreased compared to the reference configuration.

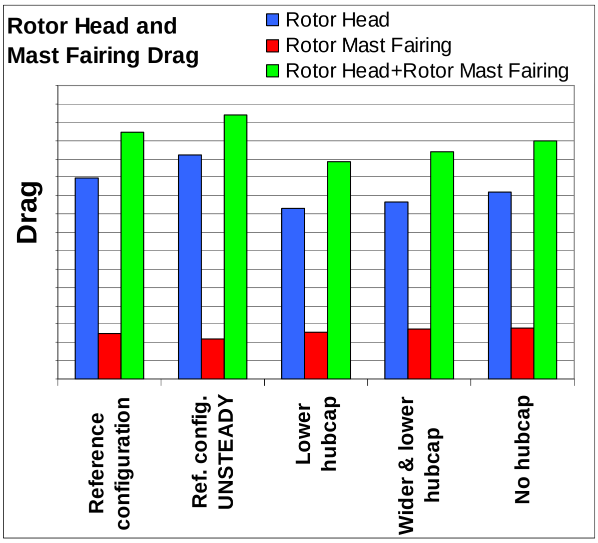

Figure 22: rotor head and mast faring drag (wind frame)

The 55mm lower and 100mm wider hubcap configuration creates a drag in between the reference configuration and the lower hubcap configuration. In contrast to the expectation that increasing the size of the hubcap would increase the lift, the results show that the lift is similar to the reference configuration. The reduction of the hubcap chamber counterbalances the increase of its lifting surface.

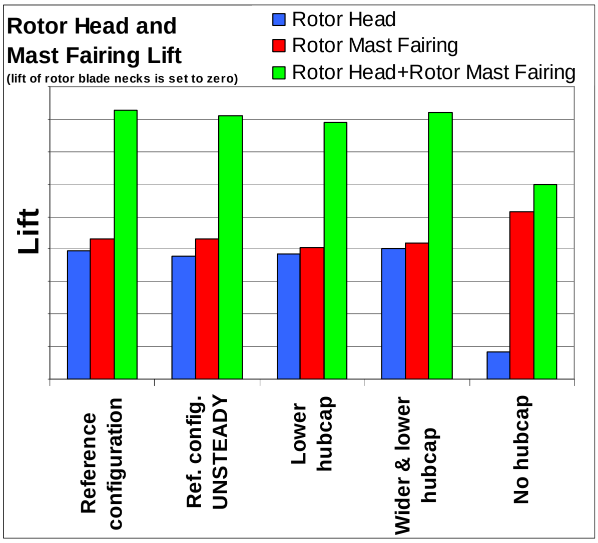

Figure 23: rotor head and mast fairing lift (wind frame, without rotor blade necks)

Figure 24 and Figure 25 show the pressure distribution as well as iso-surfaces of the kinematic vorticity for the steady and unsteady computation of the reference configuration. It is here evident the missing swirl in the rotor head wake of the non-rotating simulation and the asymmetry between the advancing and retreating blades in the rotating simulation.

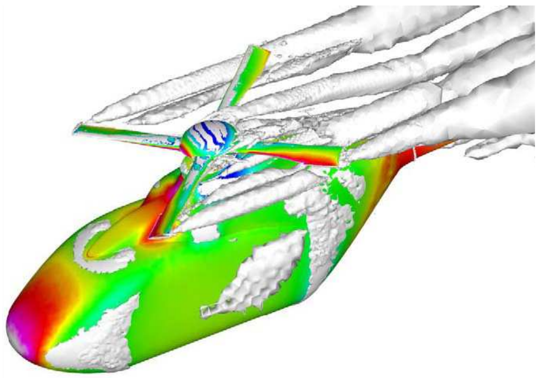

Figure 24: steady state computation of the reference configuration: pressure distribution and iso-surface of the kinematic vorticity

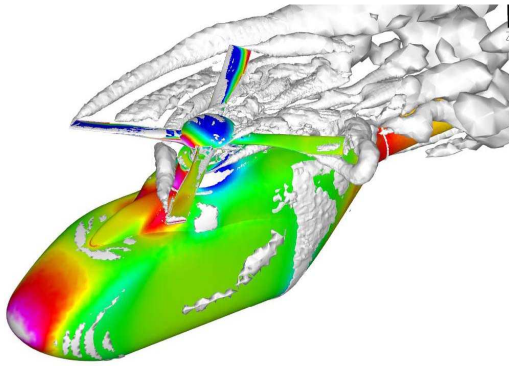

Figure 25: unsteady computation of the reference configuration: pressure distribution and iso-surface of the kinematic vorticity

CONCLUSION AND OUTLOOK

Two different numerical studies aiming at studying rotor head aerodynamics with two different flow solvers, one following a structured and the other an unstructured approach, are presented. Besides the results about different rotor head geometry designs, developed during the studies to improve the rotor head aerodynamics in terms of drag, lift and/ or power, different modelling approaches are applied and compared to each other.

Both analysis lead to a good understanding of the drag and lift contribution of different sub-components to the overall drag and lift as well as the interference effects between the rotor head components.

The construction height and the cross section distribution are identified as important parameters for the drag of the rotor blade necks. A computation with rotating rotor head should be performed to determine the drag of the blade necks. With simplifications such as computing with only one rotating rotor blade or neglecting the cyclic pitch motion of the rotor blade still reasonable results in terms of drag are achieved especially for the outboard region of the rotor blade necks. As far as the drag of the rotor head mast and inboard elements is concerned also steady state computations deliver meaningful results.

The prediction of lift turned out to be more challenging than the drag. Computing without rotor head rotation, omitting the cyclic pitch motion of the rotor blade necks or computing with one rotating rotor blade only, show significantly different results for the time-dependant aerodynamic characteristics of the rotor head components. The most complex configuration with five rotating rotor blade necks including the cyclic pitch motion therefore seems to be the most suitable approach.

To derive a benefit for the complete helicopter out of the results about the isolated rotor head, further work is necessary. Specifically the investigation of the rotor head in the flow field around the helicopter cabin and within the rotor downwash seems to be necessary. In this way also the important interference drag, occurring when the rotor head is placed on the cabin, will be addressed in addition to the direct parasite drag of the rotor head, which was the specific focus of this paper.

For the global helicopter benefit assessment of the different rotor head geometries the aerodynamic characteristics computed in the CFD studies are evaluated with a common helicopter performance tool combining drag, lift and power required to a final mission performance. This investigation is not presented in this paper.

ACKNOWLEDGEMENTS

The authors would like to thank the German ministry of Economy and Labour (BMWA) for its funding in the framework of ECO-HC (grant 20H0803).

REFERENCES

[1] Kroll, N., Eisfeld, B., and Bleecke, H.M. “The Navier-Stokes Code FLOWer”, volume 71 of Notes on Numerical Fluid Mechanics, pages 58-71. Vieweg, Braunschweig, 1999.

[2] Borie, S.; Mosca, J.; Sudre, L.; Benoit, C.; Péron, S.: Influence of Rotor Wakes on Helicopter Aerodynamic Behaviour. In: Proceedings of the 35th European Rotorcraft Forum, Hamburg, Germany, September 22nd-25th, 2009.

[3] F. Le Chuiton, T. Kneisch, S. Schneider and Ph. Krämer “Industrial validation of numerical aerodynamics about rotor heads: towards a design optimisation at EUROCOPTER”, Proceedings of the 35th European Rotorcraft Forum, Hamburg, Germany, September 22nd-25th, 2009.

[4] Gerhold, T.; Galle, M.; Friedrich, O.; Evans, J.: Calculation of Complex Three-Dimensional Configurations Employing The DLR TAU-Code. AIAA-97-0167, 1997.

[5] Schwamborn, D.; Gerhold, T.; Heinrich R.: The DLR Tau-code: Recent Applications In Research And Industry. In: Proceeding of ECCOMAS CFD 2006, Egmond aan Zee, Netherlands, September 5th-8th, 2006.

[6] Schwarz, T.: The Overlapping Grid Technique For The Time Accurate Simulation of Rotorcraft Flows. Proceedings of the 31st European Rotorcraft Forum, September 2005

[7] Kroll, N.; Rossow, C.-C.; Becker, K.; Thiele, F.: The MEGAFLOW Project. In: Aerospace Science and Technology, Vol. 4, 2002, pp. 223-237